Analytical study of post-closure behaviour of a deep spherical cavity in a dilatant viscoplastic rock mass

Yufeng Sun, Henry Wong, Benoit Pardoen, F. Deleruyelle, Nathalie Dufour, Denis Branque, Chin Jian Leo

Analytical study of post-closure behaviour of a deep spherical cavity in a dilatant viscoplastic rock mass

Y. Sun[1], H. Wong[1*], B. Pardoen[1], F. Deleruyelle[2], N. Dufour[3], D. Branque[1], C. Leo[4]

[1]LTDS (UMR- CNRS 5513), Université de Lyon, ENTPE, rue Maurice Audin, 69120 Vaulx-en-Velin, France.

[2]IRSN, PRP-DGE, SEDRE, UEMIS, Fontenay-aux-Roses, France

[3]CEREMA – DTerMed, Aix-en-Provence, France

[4]School of Computing Engineering and Mathematics, Western Sydney University, Penrith, Australia

[*]*Correspondence*： KwaiKwan.WONG@entpe.fr

Abstract

The long-term stability of an underground deep cavity involves a lot of complex time-dependent mechanical processes. This paper presents an analytical approach for the post-closure behaviour of a deep cavity inside a dilatant viscoplastic rock mass considering three stages: (1) excavation, (2) free convergence and (3) backfill contact and post-closure. The viscoplasticity is modelled by means of a linear Norton-Hoff's law, and the dilation is incorporated by assuming that the volumetric plastic strain rate is a simple function of the equivalent deviatoric plastic strain. The analytical model proposed in this paper completes a previous work of the authors by adding the consideration of the dilatant behaviour of the rock mass. After presenting the analytical developments, a few numerical examples are presented to illustrate the applicability of the model. In particular, a parametric study shows the influence of key parameters such as dilation parameter, backfill stiffness, viscosity and delay of contact between the rock mass and the internal backfill. This analytical model provides a useful benchmark for complex numerical simulations as well as a useful tool for quick preliminary studies.

Keywords: Viscoplasticity; Dilation; Deep cavity; Laplace transform; Quasi-analytical solution; Post-closure

1. Introduction

Deep cavity closure is an important issue in the geotechnics of underground works, such as mining industry (Afrouz, 1990), oil and gas extraction (Bérest et al., 2001; Cosenza and Ghoreychi, 1999), and radioactive waste disposal design (Cornet and Dabrowski, 2018; Hudson et al., 2001). Numerous works have already studied this important issue, but most of them require sophisticated modelling and advanced numerical tools (Chijimatsu et al., 2005; Liedtke and Bleich, 1985; Pardoen et al., 2015; Rutqvist et al., 2009) to take into account the exact geometry, detailed stages of construction as well as the complexity of the material behaviours. However, these numerical results are generally difficult to interpret and also need some simplified analytical solutions to check their validity.

Thus, some analytical models have also been performed to provide solutions based on idealised conditions, defined by a

set of simplifying assumptions (geometry, stress field, material behaviour, etc.). In our previous papers (Dufour et al., 2009; Wong et al., 2008a, 2008b), we focused on a quasi-analytical approach of the post-closure behaviour of a cylindrical or spherical cavity drilled into a poro-elastic or poro-viscoelastic medium and submitted to a very simplified scenario (sudden application of the lithostatic stresses on the backfill after lining failure). A solution accounting for a more realistic (but still simplified) life cycle of the tunnel has been developed by Dufour et al. (2012) in the particular case of poro-elasticity. On the other hand, Cornet et al. (2017, 2018) used both analytical and numerical modelling to study the nonlinear viscoelastic closure of salt cavities subjected to a combined pressure and shear stress load in the far field. Inelastic strains of deep rocks under loading, which have been experimentally observed (Chiarelli et al., 2003; Gatelier et al., 2002; Zhou et al., 2011), have been taken into account by considering an elastoplastic behaviour of the rock mass (Carranza-Torres and Zhao, 2009; El Jirari et al., 2020; Li et al., 2021). However, it is worth noting that many rocks, in the long-term, exhibit time-dependent irreversible strains once the applied stress deviator goes beyond a certain threshold, which has been demonstrated experimentally by several authors for different types of rocks (Boidy et al., 2002; Changa and Zoback, 2009; Gasc-Barbier et al., 2004; Jin and Cristescu, 1998; Lockner, 1993; Tang et al., 2020). In many cases, the long-term creep response due to material viscosity is described using viscoplastic theory (Zhou et al., 2008), which is used by many authors to simulate the time-dependent responses of underground structures (Giraud and Rousset, 1996; Kazmierczak et al., 2007; Malan, 2002; Pardoen and Collin, 2017). Nonetheless, these non-linear modellings generally require sophisticated computational tools to obtain solutions and do not easily lend themselves to analytical approaches. Analytical models, however, are very useful to obtain quick order-of-magnitude estimates, as well as a better understanding of the intervening physical phenomena (thanks to the explicit equations) or to check the validity of more sophisticated numerical models based on idealised limiting cases. Nguyen-minh and Pouya (1992) provided an approximate closed-form solution in the case of an unlined tunnel by assuming that the surrounding rock mass obeys an elastically incompressible Norton-Hoff's creep law. Cosenza and Ghoreychi (1999) analytically dealt with the long-term behaviour of a spherical cavity inside a saturated poro-viscoplastic rock mass in the limiting case of the stationary state, neglecting transitional stages. Bui et al. (2014) then proposed an analytical approach for the poro-viscoplastic behaviour of a deep tunnel in different stages of a simplified life cycle.

It appears that the viscoplastic volumetric strain has not been considered in these works. Indeed, it can be noticed that very few analytical models take into account the effect of dilatancy of the rock mass in the post-closure behaviour of the underground structure, although it has been experimentally evidenced (Ribacchi, 2000; Yoshinaka et al., 1998). The irreversible volumetric strains impact essentially on the stress and displacement fields, as well as on the extent of the excavation-damaged zone (EDZ) in which important irreversible strains or damage occur. In such situations, creep and dilatancy of the rock mass are two significant factors that both need to be considered in a reliable modelling approach.

In this paper, we present an analytical approach for the mechanical behaviour of a deep spherical cavity excavated in a dilatant viscoplastic rock mass, accounting for three stages of a simplified life cycle: (i) excavation; (ii) free convergence without support and (iii) convergence partially restrained by a backfill. The rock mass is supposed to be elastically incompressible (i.e. Poisson's ratio $\nu = 0.5$) and to obey a simplified "linearized" (i.e $n = 1$ in Eq. (8) below) Norton Hoff's law without hardening, nor creep-threshold. Note that according to Zhang et al. (2010), such simplifying assumptions seem nevertheless to be acceptable for a clay rock.

In order to obtain an analytical solution, the in situ stress field and material behaviour are supposed to be homogeneous and isotropic and a perfectly spherical shape for the cavity is assumed. Stress invariance in the horizontal direction is an assumption consistent with that of an infinite medium. Stress invariance relative to depth is valid for deep tunnels for which the in situ stresses at near field, where plastic strains intervene, deviate little from that at the depth of tunnel axis. Further away, only elastic strains intervene and the heterogeneity of initial stress has no impact on the results. Deviation from the idealised stress isotropy and homogeneity or the perfect spherical symmetry invariably occur in real situations, making the model predictions approximative. However, such approximate estimates are still useful both at the prelimary design stage to obtain approximate quantitative estimates and at the detailed design stage to check complex numerical simulations which can go wrong in numerous ways. Deviations from the ideal case depend on in situ conditions and it is difficult to generalise. Careful interpertations are required in each individual case.

For the viscoplastic dilatancy, inspired by classical plasticity based on experimental observations, we assume the volumetric strain rate to be a linear function of the equivalent deviatoric strain rate. The stress and displacement fields are firstly determined in the Laplace transform space, followed by a numerical inversion using the Stehfest algorithm (Stehfest, 1970) to obtain the corresponding quantities in the time space. A few numerical examples are shown to illustrate the consistency of the solution and to get some useful physical insights. It is thought that the developments shown here can be a useful example for constructing analytical solutions for other engineering problems.

2. Description of the problem

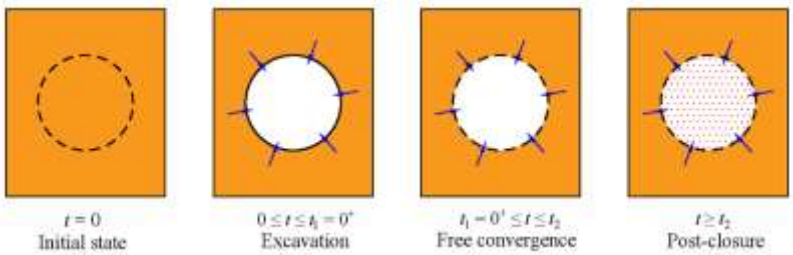

Fig. 1. Simplified life cycle of a deep cavity: (1) excavation; (2) free convergence; (3) backfill contact and post-closure.

The life cycle of an underground cavity is idealized as 3 stages schematized in Fig. 1. To simplify the problem presentation, At time t = 0 consider an non-deformed initial reference configuration for the host rock, which is supposed to be in equilibrium with the geostatic pressure with zero displacements and strains.

It is assumed that the cavity is at a great depth so that the stress heterogeneity in the surrounding rock mass can be neglected. Decompression due to excavation is the main driving force in our problem; the effects of gravity is accounted for in the constitution of initial stress and no longer intervene in subsequent stages in a quasi-static analysis. The first stage ($0 \leq t \leq t_1 = 0^+$) is related to the excavation of a deep cavity inside the rock mass. Since the time required for excavation is very short compared to other stages, the excavation is considered as an instantaneous process. The second stage corresponds to the free convergence of the surrounding rock mass, in the absence of any support. It is assumed here that either the rock mass is self-stable, or that the lining installed immediately after excavation deteriorates rapidly compared to the duration of the free convergence stage, so that the duration of the effective support is negligible. Hence, this period of free convergence starting at time $t_1 = 0^+$ continues until a certain time t_2. At this instant, the cavity wall is supposed to come into contact with a linear elastic backfill. Afterwards, the cavity wall continues to converge at a slower speed due to the confinement effect of the backfill.

3. General framework and resolution method

In the following, the tensor and vector quantities are written in bold and the scalars are denoted in normal font. Spherical symmetry conditions are assumed, resulting in the dependence of all physical quantities on only two variables, the radial coordinate r and time t. Under these conditions and using the spherical coordinate system, the stress and strain tensors are diagonal (tensile stresses and strains taken to be positive) with equal angular components and the displacement field is purely radial:

$$\boldsymbol{\sigma} = \begin{bmatrix} \sigma_r & & \\ & \sigma_\theta & \\ & & \sigma_\theta \end{bmatrix} ; \boldsymbol{u} = \begin{pmatrix} u \\ 0 \\ 0 \end{pmatrix} ; \boldsymbol{\varepsilon} = \begin{bmatrix} \partial_r u & & \\ & u/r & \\ & & u/r \end{bmatrix} \quad (1)$$

where $u = (r, t)$ is the radial displacement. The volumetric strain ϵ is related to the radial displacement u by:

$$\epsilon \equiv tr(\boldsymbol{\varepsilon}) = \frac{\partial u}{\partial r} + 2\frac{u}{r} \quad (2)$$

The unique non-trivial equilibrium equation in spherical symmetry writes:

$$\sigma_r - \sigma_\theta = -\frac{r}{2}\frac{\partial \sigma_r}{\partial r} \quad (3)$$

Under the assumption of small strains, the strain tensor can be decomposed into its elastic and visco-elastic parts, denoted by superscripts ^{e} and ^{vp}, respectively:

$$\boldsymbol{\varepsilon} = \boldsymbol{\varepsilon}^e + \boldsymbol{\varepsilon}^{vp} \quad (4)$$

3.1 Elastic constitutive equations

Under spherical symmetry, the mean stress σ_m and deviatoric stress tensor $\boldsymbol{s}$ write:

$$\sigma_m \equiv \frac{1}{3}\mathrm{tr}(\boldsymbol{\sigma}) = \frac{1}{3}(\sigma_r + 2\sigma_\theta) \;;\; \boldsymbol{s} \equiv \mathrm{dev}(\boldsymbol{\sigma}) = \frac{\sigma_r - \sigma_\theta}{3}\begin{bmatrix} 2 & & \\ & -1 & \\ & & -1 \end{bmatrix} \tag{5}$$

where $\boldsymbol{I}$ is the second-order identity tensor. According to Eq. (5) and the relation $\sigma_r > \sigma_\theta$ (due to the decompression), the Von Mises equivalent stress q can be written as:

$$q \equiv \sqrt{(3/2)\boldsymbol{s}:\boldsymbol{s}} = |\sigma_r - \sigma_\theta| = \sigma_r - \sigma_\theta \tag{6}$$

Substituting Eq. (3) into Eq. (6), the expression of q can be rewritten as: $q = -(r/2)\partial_r\sigma_r$. This paper will be limited to the case of elastic incompressibility, that is to say $v = 0.5$, which implies that the bulk modulus of the rock mass will tend to infinity (i.e. $K \to \infty$) and the shear modulus G is linked to Young's modulus E by $G = E/3$. This amounts to neglect the elastic volume changes relative to their viscoplastic counterparts. Thus, the simplified rate form of the Hooke's law writes, on account of spherical symmetry and Eqs. (1) and (5):

$$\dot{\boldsymbol{\varepsilon}}^e = \frac{1}{2G}\dot{\boldsymbol{s}} = \frac{\dot{\sigma}_r - \dot{\sigma}_\theta}{E}\begin{bmatrix} 1 & & \\ & -1/2 & \\ & & -1/2 \end{bmatrix} \tag{7}$$

where a dot above a variable indicates the partial derivative with respect to time.

3.2 Viscoplastic constitutive equations

Based on experimental investigations, the creep behaviour of a relatively large class of geomaterials with low volumetric dilatancy can be adequately described by the following creep law based on the overstress concept of Perzyna (1966):

$$\dot{\boldsymbol{\varepsilon}}^{vp} = \frac{\langle q - \sigma_s \rangle^n}{\eta}\boldsymbol{m} \tag{8}$$

where $\langle x \rangle = x$ for $x \geq 0$ and $\langle x \rangle = 0$ for $x < 0$, the equivalent shear stress q is defined in (6), σ_s is a positive stress threshold so that $q < \sigma_s$ defines an elastic domain with zero creep strain rate ($\dot{\boldsymbol{\varepsilon}}^{vp} = 0$), η is the dynamic viscosity, the positive exponent n allows to account for some form of non-linearity. Finally, the tensor $\boldsymbol{m}$ (normalised or not) defines the direction of $\dot{\boldsymbol{\varepsilon}}^{vp}$. In essence, Eq. (8) says that the viscoplastic strain rate is zero when the stress point is inside an elastic domain defined by $q - \sigma_s \leq 0$, and increases as the stress point moves further away from the elastic domain.

A commonly adopted assumption is to identify the tensor $\boldsymbol{m}$ with the deviatoric stress tensor ($\boldsymbol{m} = \boldsymbol{s}$) which implies isochoric creep strain since then $tr(\dot{\boldsymbol{\varepsilon}}^{vp}) = tr(\boldsymbol{s}) = 0$. This assumption, initially adopted for metals, leads to a simple model applicable to a class of materials with small volume change (metals, saturated clays, etc.).

Many experimental investigations have been performed to access the various material constants relative to the above constitutive law, in particular the stress threshold σ_s. While laboratory investigations of relatively short durations (commonly a few weeks to

exceptionally a few years) indicate positive values, an assumption that makes the analytical resolution much easier is to assume that σ_s may approach zero for very long term behaviour. Since the identification of the stress threshold below which creep ceases can be particularly difficult for materials such as clays Zhang et al. (2010), this assumption can be seen as a simple and conservative one to assess the maximum extension of the damaged zone likely to develop in the long term around a cavity. In this paper, attention is focused on building an analytical model to study the case of zero stress threshold: $\sigma_s = 0$. Consistently with the objective of developing an analytical solution, we will also assume a unit stress exponent, $n = 1$, in the sequel.

Concerning the non-accounting of dilatancy by taking $\boldsymbol{m} = \boldsymbol{s}$, this assumption which seems satisfactory in some cases like salt becomes questionable and may lead to unacceptable errors for other geomaterials. A volume dilatancy is introduced to remediate this defect. To this end, the viscoplastic strain rate tensor is expressed as the sum of a volumetric and a deviatoric components:

$$\dot{\boldsymbol{\varepsilon}}^{vp} = \dot{\boldsymbol{\varepsilon}}_q^{vp} + \left(\frac{\dot{\varepsilon}_v^{vp}}{3}\right)\boldsymbol{I} \tag{9}$$

where $\dot{\boldsymbol{\varepsilon}}_q^{vp}$ is defined by (8) with $\boldsymbol{m} = \boldsymbol{s}$ and $\sigma_s = 0$. For future reference, let us introduce the scalar invariant named "*equivalent deviatoric viscoplastic strain rate*" by the relation: $\dot{\gamma}_q^{vp} = \left\|\dot{\boldsymbol{\varepsilon}}_q^{vp}\right\|$. Note that for second-order symmetric tensors: $\|\boldsymbol{t}\| = \sqrt{\boldsymbol{t}:\boldsymbol{t}} = \sqrt{t_{ij}t_{ij}}$.

Under the condition of spherical symmetry and on account of the previous assumptions and notations, the deviatoric component of the viscoplastic strain rate tensor can be written as:

$$\dot{\boldsymbol{\varepsilon}}_q^{vp} = \frac{\sigma_r - \sigma_\theta}{\eta}\begin{bmatrix} 1 & & \\ & -1/2 & \\ & & -1/2 \end{bmatrix} \tag{10}$$

Concerning the volumetric component, it is found in only a few creep models. The viscoplastic models proposed by Pellet et al. (2005) and by Bui et al. (2017), which also account for damage behaviour, are two examples. Their construction is based on a thermodynamic approach, in which the strain rate tensor is obtained by differentiating a dissipation potential. These complex models cannot yield analytical solutions, even with simplified geometry and construction stages. In this paper, the new model proposed is adopted from a family of classical plastic models in which the volumetric plastic strain rate $\dot{\varepsilon}_v^{vp}$ is expressed as a simple function of the equivalent deviatoric plastic strain rate $\dot{\gamma}_q^{vp}$ (Zhao et al., 2020). In the context of underground structures in soil or rock masses, deformations are mainly due to tangential relative displacements of non-smooth interfaces or between grains at the microscale (Pardoen et al., 2020), inducing normal displacements, which is the physical origine of volumetric dilation. In consequence, it is reasonable to assume a correlation between volumetric dilation and shear strain. Note that this volumetric dilation has important impact on the shear resistance and the plastic behaviour among geomaterials, which is often described by some form of volumetric hardening law, such as the classic Cam-Clay model. A more detailed account on different possible correlations between $\dot{\varepsilon}_v^{vp}$ and $\dot{\gamma}_q^{vp}$ can be found in Yu (2006). The simplest correlation is a linear relation, which is consistent

with the objective of building an analytical model. We therefore assume the following linear form defined by a dilation parameter α_0:

$$\dot{\varepsilon}_v^{vp} = \alpha_0 \, \dot{\gamma}_q^{vp} \tag{11}$$

It should be noted that Eq. (11) can also take the equivalent incremental form $d\varepsilon_v^{vp} = \alpha_0 d\gamma_q^{vp}$. The pertinence of this simplified dilatancy rule has been confirmed by Tian et al. (1994) through drained creep tests on marine sediments at lower stress level, while it has to be replaced by a piecewise linear relation at higher stress level. Several authors (Sekiguchi, 1973; Wang and Yin, 2014) also proposed some other different relationships between $d\varepsilon_v^{vp}$ and $d\gamma_q^{vp}$.

Based on Eqs. (6), (10) and (11), the volumetric plastic strain rate in tensor form $\frac{\dot{\varepsilon}_v^{vp}}{3}\boldsymbol{I}$ writes:

$$\frac{\dot{\varepsilon}_v^{vp}}{3}\boldsymbol{I} = \alpha \frac{\sigma_r - \sigma_\theta}{\eta}\boldsymbol{I}; \quad \alpha = \frac{\alpha_0}{\sqrt{6}} \tag{12}$$

Therefore, the total viscoplastic strain rate can be written as follows by the sum of Eqs. (10) and (12):

$$\dot{\boldsymbol{\varepsilon}}^{vp} = \left(\frac{\dot{\varepsilon}_v^{vp}}{3}\right)\boldsymbol{I} + \dot{\boldsymbol{\varepsilon}}_q^{vp} = \frac{\sigma_r - \sigma_\theta}{\eta}\begin{bmatrix} 1+\alpha & & \\ & \alpha - 1/2 & \\ & & \alpha - 1/2 \end{bmatrix} \tag{13}$$

Finally, eliminating the strains from Eqs. (1), (7) and (13), we get the following system of partial differential equations:

$$\frac{\partial \dot{u}}{\partial r} = \frac{1}{E}(\dot{\sigma}_r - \dot{\sigma}_\theta) + \frac{1+\alpha}{\eta}(\sigma_r - \sigma_\theta) \tag{14-a}$$

$$\frac{\dot{u}}{r} = -\frac{1}{2E}(\dot{\sigma}_r - \dot{\sigma}_\theta) + \frac{\alpha - 1/2}{\eta}(\sigma_r - \sigma_\theta) \tag{14-b}$$

To summarize, the problem is governed by a system of 3 equations (3), (14a) and (14b) on the three variables u, σ_r and σ_θ.

3.3 Resolution method

Except for the first stage (instantaneous excavation) whose solution is trivial, the general resolution method consists at first transforming all the variables into the Laplace transform space by $\bar{f}(r,s) = L\{f(r,t)\} = \int_0^\infty f(r,t)e^{-st}dt$, leading to a system of ordinary differential equations (ODE's) from which the unknown variables are determined. This is followed by the inversion of the solution obtained in the transformed space back to the real time space. Considering that this last step cannot be done analytically when the functions are too complex, a numerical inversion according to the Stehfest algorithm (Stehfest, 1970) is adopted:

$$f(r,t) = L^{-1}\left[\bar{f}(r,s)\right] \cong \frac{ln2}{t}\sum_{n=1}^{N}\xi_n \bar{f}\left(r, n\frac{ln2}{t}\right) \tag{15}$$

$$\xi_n = (-1)^{n+\frac{N}{2}} \sum_{k=Int\left(\frac{n+1}{2}\right)}^{\min(n,\frac{N}{2})} \frac{k^{\frac{N}{2}}(2k)!}{\left(\frac{N}{2}-k\right)!\,k!\,(k-1)!\,(n-k)!\,(2k-n)!} \tag{16}$$

where $Int(x)$ means the integer part of x, N is an even positive integer; note that the coefficients ξ_n verify the identity $\sum_{n=1}^{N}\frac{\xi_n}{n} = 1$, as pointed out by Dufour et al. (2012).

3.4. Normalization of variables

In order to better illustrate the physical connection between different parameters and above all to give a compact presentation, the variables are normalized relative to their respective characteristic values according to the following scheme:

$$\Sigma_r = \frac{\sigma_r}{P_\infty};\ \Sigma_\theta = \frac{\sigma_\theta}{P_\infty};\ U = \frac{E}{P_\infty}\frac{u}{a};\ r' = \frac{r}{a};\ t' = \frac{t}{T_0};\ t_1' = \frac{t_1}{T_0};\ t_2' = \frac{t_2}{T_0};\ p_R' = \frac{p_R}{P_\infty};\ K_R' = \frac{K_R}{E} \tag{17}$$

where Σ_r, Σ_θ, U, r', t' are respectively the normalized stresses, radial displacement, radial coordinate and time, P_∞ is the geostatic pressure; a is the cavity radius; p_R is the backfill pressure; K_R is the backfill stiffness (see Eq. (A1)); T_0 is taken as the characteristic time of creep, defined as $T_0 = \frac{\eta}{E}$, which is identical to the characteristic relaxation time due to the elastic incompressibility assumption. The relation between the two characteristic times can be found in Bui et al. (2014). The unknowns of the problem are now $U(r',t')$, $\Sigma_r(r',t')$ and $\Sigma_\theta(r',t')$.

4. First stage: excavation of cavity ($0 \le t \le t_1 = 0^+$)

As mentioned above, the first stage corresponds to an instantaneous excavation of a spherical cavity inside an infinite domain.

4.1 Initial and boundary conditions

The initial state at $t' = 0$ is used as the initial reference configuration in which the rock mass is under mechanical equilibrium and characterized by a homogeneous isotropic stress field equal to the geostatic pressure P_∞. Moreover, the displacements and strains in this initial state are null, Therefore, the initial conditions at $t' = 0$ are:

$$\Sigma_r(r',0) = \Sigma_\theta(r',0) = -1;\ U(r',0) = 0 \tag{18}$$

During excavation, the radial stress σ_r at the cavity wall jumps instantaneously from $-P_\infty$ to zero, while the radial displacement and stress at infinity remain at their initial values since the perturbation due to excavation of a finite-size cavity cannot propagate to infinity. Therefore:

$$\Sigma_r(1,0^+) = 0;\ \ \Sigma_r(\infty,0^+) = -1;\ U(\infty,t') = 0; \tag{19}$$

4.2 Analytical solution

With the above initial conditions (18) and boundary conditions (19), the analytical solution in time domain for this stage can be deduced. As the excavation occurs instantaneously, the creep (i.e. viscoplastic) strains of a finite rate have no time to develop and therefore remain null; only elastic strains intervene. Since this resolution is classical, the computations are not shown. They can be found for example in (Dufour et al., 2012). The solution for the displacement and stress fields is given below:

$$U^+(r') = -\frac{3}{4}r'^{-2};\quad \Sigma_r^+(r') = -\left[1 - r'^{-3}\right];\ \Sigma_\theta^+(r') = -\left[1 + \frac{1}{2}r'^{-3}\right] \tag{20}$$

The elastic strain field can be obtained by Eq. (1).

5. Second stage: free convergence without support ($t_1 = 0^+ \leq t \leq t_2$)

5.1 Initial and boundary conditions

Time evolution of various field quantities are supposed to be continuous. Their initial values for this second stage (i.e. at time $t_1' = 0^+$) are therefore given by the solution of Stage 1 in Eq. (20). During this stage, the radial stress at the cavity wall and that at far field both remain constant, respectively equal to zero and to the geostatic pressure, or in terms of normalized quantities: $\Sigma_r(1, t') = 0$; $\Sigma_r(\infty, t') = -1$. In the Laplace transform space, we have:

$$\bar{\Sigma}_r(1, s) = 0\ ;\ \bar{\Sigma}_r(\infty, \mathrm{s}) = -\frac{1}{s} \tag{21}$$

5.2 Quasi-analytical solution

In terms of the normalized variables introduced in (17), Eqs. (14) can be rewritten as:

$$\frac{\partial \dot{U}}{\partial r'} = \dot{\Sigma}_r - \dot{\Sigma}_\theta + (1 + \alpha)(\Sigma_r - \Sigma_\theta) \tag{22-a}$$

$$\frac{\dot{U}}{r'} = -\frac{\dot{\Sigma}_r - \dot{\Sigma}_\theta}{2} + \left(\alpha - \frac{1}{2}\right)(\Sigma_r - \Sigma_\theta) \tag{22-b}$$

where a dot above a variable now represents the partial derivative relative to t'. The equilibrium equation (3) in terms of normalized variables writes, respectively in the time domain and Laplace domain:

$$\Sigma_r - \Sigma_\theta = -\frac{r'}{2}\frac{\partial \Sigma_r}{\partial r'};\quad \bar{\Sigma}_r - \bar{\Sigma}_\theta = -\frac{r'}{2}\frac{\partial \bar{\Sigma}_r}{\partial r'} \tag{23}$$

Applying the Laplace transform to Eqs. (22) and eliminating the tangential stress $\bar{\Sigma}_\theta$ using Eq. (23), we get the following two equations on the two variables U and Σ_r:

$$s\frac{\partial \bar{U}}{\partial r'} = -\frac{s + 1 + \alpha}{2}r'\frac{\partial \bar{\Sigma}_r}{\partial r'} + \left(\frac{\partial U^+}{\partial r'} - \Sigma_r^+ + \Sigma_\theta^+\right) \tag{24}$$

$$s\frac{\bar{U}}{r'} = \frac{s + 1 - 2\alpha}{4}r'\frac{\partial \bar{\Sigma}_r}{\partial r'} + \left(\frac{U^+}{r'} + \frac{\Sigma_r^+ - \Sigma_\theta^+}{2}\right) \tag{25}$$

Note that the expressions inside the two parentheses involving initial values at $t_1' = 0^+$ are both zero, on account of (20).

Dividing the difference between Eqs. (24) and (25) by r', followed by an integration relative to r' leads to:

$$s\frac{\bar{U}}{r'} = -\frac{3(s+1)}{4}\bar{\Sigma}_r + A(s) \tag{26}$$

where $A(s)$ is an integration constant. Eliminating $s\frac{\bar{U}}{r'}$ between Eqs. (25) and (26) leads to the following equation on $\bar{\Sigma}_r$:

$$r'\frac{\partial\bar{\Sigma}_r}{\partial r'} + \Lambda(s)\bar{\Sigma}_r = \frac{4A(s)}{s+1-2\alpha};\ \ \Lambda(s) = \frac{3(s+1)}{s+1-2\alpha} \tag{27}$$

Solving the linear differential Eq. (27) and considering the boundary conditions (21), we obtain the solution of $\bar{\Sigma}_r$:

$$\bar{\Sigma}_r = -\frac{1}{s}\left[1 - r'^{-\Lambda(s)}\right] \tag{28}$$

$\bar{\Sigma}_\theta$ and $\bar{U}$ can then be calculated, respectively, by substituting the above equation into Eqs. (23) and (25):

$$\bar{\Sigma}_\theta = -\frac{1}{s}\left[1 + \left(\frac{\Lambda(s)}{2} - 1\right)r'^{-\Lambda(s)}\right] \tag{29}$$

$$\bar{U} = -\frac{3}{4}\left(\frac{1}{s} + \frac{1}{s^2}\right)r'^{-(\Lambda(s)-1)} \tag{30}$$

Note that when $\alpha = 0$ (therefore $\Lambda(s) = 3$), the solution above is consistent with the case of a non-dilatant viscoplastic rock mass. The quasi-analytical solution in the time-domain can be obtained by numerical inversion of (28)-(30) using the Stehfest algorithm. However, it is interesting to note that entirely explicit expressions can be obtained for quantities at the cavity wall ($r' = 1$):

$$\Sigma_r(1, t') = 0 \tag{31-a}$$

$$\Sigma_\theta(1, t') = \mathcal{L}^{-1}\left[-\frac{3(s+1)}{2s(s+1-2\alpha)}\right] = -\frac{3}{2(1-2\alpha)}\left[1 - 2\alpha e^{-(1-2\alpha)t'}\right] \tag{31-b}$$

$$U(1, t') = -\frac{3}{4}(1 + t') \tag{31-c}$$

Note that the parameter α does not intervene on the cavity wall convergence. This is due to the idealised geometry (spherical symmetry and infinite domain) and the linear constitutive model assumed. This fact can be paralleled to the famous result that an infinite homogeneous isotropic linear elastic medium outside a spherical/cylindrical cavity when subject to an arbitrary temperature field shows zero displacement at the cavity wall, despite an outward displacement induced by thermal dilation at every other point (Berest and Weber, 1998).

At time $t' = t'_2$, the cavity wall is supposed to enter into contact with a backfill, which marks the end of Stage 2 of free convergence.

6. Third stage: backfill and post-closure ($t_2 \leq t \leq \infty$)

At $t' = t'_2$, the third stage begins and the convergence of the cavity wall continues, while partially restrained by the presence of a backfiill in contact with the cavity wall. To compute the reaction of the backfill on the converging cavity wall, we assume that its mechanical behaviour can be approximated by a linear elastic constitutive law. The resolution of this stage constitutes the

main part of this paper. Detailed computations are reported in Appendix A.

6.1 Initial and boundary conditions

The equations to be solved are Eqs. (24) and (25) in the transformed domain. However, for the present Stage 3, the initial values $(U^+, \Sigma_r^+, \Sigma_\theta^+)$ at $t = 0^+$ in these equations have to be replaced by the corresponding values of $(U, \Sigma_r, \Sigma_\theta)$ at the end of Stage 2 (i.e. at time $t' = t_2'$), to be computed using expressions (28)-(30).

Instead of calculating the values separately of U, Σ_r and Σ_θ at $t' = t_2'$, we attempt to compute directly the expressions inside the parentheses of Eqs. (24) and (25) as a whole. The following notations are therefore introduced:

$$\Delta_r(r', t') = \left(\frac{\partial U}{\partial r'} - \Sigma_r + \Sigma_\theta\right)_{t' \le t_2'}; \quad \Delta_\theta(r', t') = \left(\frac{U}{r'} + \frac{\Sigma_r - \Sigma_\theta}{2}\right)_{t' \le t_2'} \tag{32}$$

In fact, we only need to calculate Δ_r and Δ_θ at the instant $t' = t_2'$, which we note as $\Delta_r^{(2)}(r')$ and $\Delta_\theta^{(2)}(r')$. Since it is not possible to analytically inverse the expressions (28)-(30), the Stehfest algorithm is used to obtain approximate values. The Laplace transform of $\Delta_r(r', t')$ and $\Delta_\theta(r', t')$, using (28)-(30), can be cast into the following form:

$$\bar{\Delta}_r(r', s) = A_r(s) r'^{-\Lambda(s)}; \; \bar{\Delta}_\theta(r', s) = A_\theta(s) r'^{-\Lambda(s)} \tag{33}$$

with:

$$A_r(s) = \frac{3(s+1)(1+\alpha)}{2s^2(s+1-2\alpha)}; \; A_\theta(s) = \frac{3(s+1)(2\alpha-1)}{4s^2(s+1-2\alpha)} \tag{34}$$

Moreover, introducing the notation $\bar{\Delta}_{r\theta}(r', s) \overset{\text{def}}{=} \bar{\Delta}_r(r', s) - \bar{\Delta}_\theta(r', s)$, we get from (33) and (34):

$$\bar{\Delta}_{r\theta}(r', s) = A_{r\theta}(s) r'^{-\Lambda(s)}; \; A_{r\theta}(s) = \frac{3\Lambda(s)}{4s^2} \tag{35}$$

The two quantities $\Delta_r^{(2)}$ and $\Delta_\theta^{(2)}$ in the time domain, necessary to account for the initial conditions of this Stage 3, can then be obtained:

$$\Delta_r^{(2)} = \sum_n b_n \bar{\Delta}_r(r', \tau_n) = \sum_n b_n A_{rn} r'^{-\Lambda_n} \tag{36-a}$$

$$\Delta_\theta^{(2)} = \sum_n b_n \bar{\Delta}_\theta(r', \tau_n) = \sum_n b_n A_{\theta n} r'^{-\Lambda_n} \tag{36-b}$$

$$\Delta_{r\theta}^{(2)} = \sum_n b_n \bar{\Delta}_{r\theta}(r', \tau_n) = \sum_n b_n A_{r\theta}^n r'^{-\Lambda_n} \tag{36-c}$$

where:

$$b_n = \xi_n \frac{ln2}{t_2'}; \; \tau_n = n \frac{ln2}{t_2'}; \; A_{rn} = A_r(\tau_n); \; A_{\theta n} = A_\theta(\tau_n); \; A_{r\theta}^n = A_{r\theta}(\tau_n); \; \Lambda_n = \Lambda(\tau_n)$$

Recall that the following identity, as reported in (Dufour et al., 2012), applies:

$$\sum_{n=1}^{N} \frac{b_n}{\tau_n} = \sum_{n=1}^{N} \frac{\xi_n}{n} = 1 \tag{36-d}$$

The stress boundary condition at infinity, Eq. (20), is still applicable for this stage. However, the radial stress at the cavity wall $\Sigma_r(1, t')$ will no longer be null due to the reaction from the backfill. It is linked to the normalized convergence ((i.e.

248 normalized displacement at the cavity wall) via the following condition (see Appendix A):

$$\Sigma_r(1,t') = K_R'(U(1,t') - U(1,t_2')) \tag{37}$$

249 The above condition writes, in the transformed space:

$$\bar{\Sigma}_r(1,s) = K_R^{'}\left(\bar{U}(1,s) - \frac{U(1,t_2^{'})}{s}\right) \tag{38}$$

250 **6.2 Quasi-analytical solution**

251 A translation of the time coordinate, $\tau = t' - t_2'$, is introduced to properly define the Laplace transform at Stage 3.
252 Therefore, the following fields are defined: $\widehat{U}(r',\tau) = U(r',t')$; $\widehat{\Sigma_r}(r',\tau) = \Sigma_r(r',t')$; $\widehat{\Sigma_\theta}(r',\tau) = \Sigma_\theta(r',t')$, with $\tau = 0$
253 corresponding to the beginning of this stage.

254 Taking into account the definitions (31) and notations $\Delta_r^{(2)}$ and $\Delta_\theta^{(2)}$, Eqs. (24) and (25) become:

$$s\frac{\partial\bar{\widehat{U}}}{\partial r'} = -\frac{s+1+\alpha}{2}r'\frac{\partial\overline{\widehat{\Sigma_r}}}{\partial r'} + \Delta_r^{(2)} \tag{39-a}$$

$$s\frac{\bar{\widehat{U}}}{r'} = \frac{s+1-2\alpha}{4}r'\frac{\partial\overline{\widehat{\Sigma_r}}}{\partial r'} + \Delta_\theta^{(2)} \tag{39-b}$$

255 Dividing the difference between Eqs. (39-a) and (39-b) by r', and using expressions (36-a) and (36-b), leads to:

$$s\frac{\partial}{\partial r'}\left(\frac{\bar{\widehat{U}}}{r'}\right) = -\frac{3(s+1)}{4}\frac{\partial\overline{\widehat{\Sigma_r}}}{\partial r'} + \sum_n b_n A_{r\theta}^n r'^{-(\Lambda_n+1)} \tag{40}$$

256 Integration with respect to r' gives:

$$s\frac{\bar{\widehat{U}}}{r'} = -\frac{3(s+1)}{4}\overline{\widehat{\Sigma_r}} - \beta(r') + C(s) \tag{41}$$

257 where $C(s)$ is an integration constant and $\beta(r')$ is defined by:

$$\beta(r') = \sum_n \frac{b_n A_{r\theta}^n}{\Lambda_n} r'^{-\Lambda_n} \tag{42}$$

258 Elimination of the term $s\frac{\bar{\widehat{U}}}{r'}$ between Eqs. (39-b), (41) and (42) leads to the following equation on the unique variable $\widehat{\Sigma_r}$:

$$r'\frac{\partial\overline{\widehat{\Sigma_r}}}{\partial r'} + \Lambda(s)\bar{\Sigma}_r = \frac{C(s)}{(s+1-2\alpha)/4} - \sum_n B_n(s) r'^{-\Lambda_n} \tag{43}$$

259 which admits the solution:

$$\overline{\widehat{\Sigma_r}} = \frac{C(s)}{\frac{3}{4}(s+1)} + D(s)r'^{-\Lambda(s)} + \zeta(r',s) \tag{44}$$

260 where $D(s)$ is is an integration constant and the following notations have been introduced:

$$B_n(s) = \frac{b_n}{(s+1-2\alpha)/4}\left(A_{\theta n} + \frac{A_{r\theta}^n}{\Lambda_n}\right); \quad \zeta(r',s) = \sum_n \frac{B_n(s)}{\Lambda_n - \Lambda(s)} r'^{-\Lambda_n} \tag{45}$$

261 Introducing the stress boundary condition at infinity (21-b) into Eq. (43), we get $C(s) = -\frac{3}{4}\left(\frac{s+1}{s}\right)$. $D(s)$ then can be

determined by taking into account the stress boundary condition at the cavity wall Eq. (38):

$$D(s) = -\zeta(1,s) + \gamma(s);\ \ \gamma(s) = \frac{1}{\omega + s};\ \ \omega = \frac{\frac{3}{4}K'_R}{1+\frac{3}{4}K'_R} \tag{46}$$

Hence, the complete Laplace transform solution at Stage 3 is given by:

$$\overline{\overline{\Sigma_r}} = -\frac{1}{s} + \gamma(s) r'^{-\Lambda(s)} + \sum_n B_n(s) \frac{r'^{-\Lambda_n} - r'^{-\Lambda(s)}}{\Lambda_n - \Lambda(s)} \tag{47}$$

$$\overline{\overline{\Sigma_\theta}} = -\frac{1}{s} + \gamma(s)\left(1 - \frac{\Lambda(s)}{2}\right) r'^{-\Lambda(s)} + \sum_n B_n(s) \frac{\left(1-\frac{\Lambda_n}{2}\right) r'^{-\Lambda_n} - \left(1-\frac{\Lambda(s)}{2}\right) r'^{-\Lambda(s)}}{\Lambda_n - \Lambda(s)} \tag{48}$$

$$\frac{\overline{\overline{U}}}{r'} = -\frac{3(s+1)}{4s}\left[\gamma(s) r'^{-\Lambda(s)} + \sum_n B_n(s) \frac{r'^{-\Lambda_n} - r'^{-\Lambda(s)}}{\Lambda_n - \Lambda(s)}\right] - \frac{1}{s}\beta(r') \tag{49}$$

Note that the above expressions are continuous relative to the previous stage, as shown in detail in Appendix B, ensuring the consistency of the solution. While Eq. (49) cannot be inverse-transformed analytically for an arbitrary location, this can be done for $r' = 1$ to obtain an explicit expression for the normalized displacement at the cavity wall:

$$U(1,t') = -\frac{3}{4}\left[1 + t'_2 + \left(\frac{1}{\omega} - 1\right)\left(1 - e^{-\omega(t'-t'_2)}\right)\right] \tag{50}$$

Detailed computations for getting above equation are shown in Appendix C. The normalized displacement at the cavity wall in the third stage can be decomposed into 2 parts: the first part is only the initial value at the beginning of this stage, equal to Eq. (31-c), while the second one is the evolution of the convergence expressing the simultaneous effects of creep and backfill. The convergence rate slows down continuously and the normalized displacement tends towards a final stable value: $-\frac{3}{4}\left[\frac{1}{\omega} + t'_2\right]$ at large time. Recall that $\omega = \frac{\frac{3}{4}K'_R}{1+\frac{3}{4}K'_R}$, a stiffer backfill reduces the displacement at the cavity wall as expected. And in the case of an infinitely stiff backfill ($K'_R \to \infty, \omega \to 1$), the convergence would stop in Stage 3. Moreover, the magnitude of the displacement at a given physical time t is inversely proportional to the material viscosity (via T_0). When the viscosity tends to infinity, the incompressible elastic case is restored.

Based on Eqs. (31-c) and (50), it can be seen that the time evolution of the displacement at the cavity wall, as in the previous stage, is not dependent on the dilation parameter α. Based on Eq. (37), the normalized backfill pressure (i.e. an elastic reaction to the cavity wall,) P'_R in Fig. 16 can be written as $P'_R(t') = -\Sigma_r(1,t') = -K'_R(U(1,t') - U(1,t'_2))$, and combining this relation with Eqs. (31-c) and (50) gives:

$$P'_R(t') = \frac{3K'_R}{4}\left[\left(\frac{1}{\omega} - 1\right)\left(1 - e^{-\omega(t'-t'_2)}\right)\right] \tag{51}$$

Eq. (51) shows that the backfill reaction always tends towards P_∞ at large times. This is due to the absence of stress-threshold in

the creep model, which implies that static equilibrium with zero strain rates can only be achieved with zero deviatoric stress. In consequence, equilibrium can only take place when the internal pressure at the cavity wall (supplied here by the backfill) is equal to the geostatic pressure at far field.

In Eqs. (47)-(49), there is an apparent singularity when $\Lambda_n - \Lambda(\mathrm{s})$ approaches zero. Note that in the numerical inversion using the Stehfest algorithm, at a time $t' > t'_2$, $\Lambda_n - \Lambda(\mathrm{s})$ is evaluated as $\Lambda\left(n\frac{ln2}{t'_2}\right) - \Lambda\left(m\frac{ln2}{t'-t'_2}\right)$ with $1 \le m,n \le N$ (N is the upper limit of summation in Eq. (15)) which can approach zero, hence a mathematical singularity. However, this singularity is only apparent, as the numerators also become zero and their corresponding ratios approach well-defined limits, on account of the following results:

$$\lim_{\Lambda(\mathrm{s})\to\Lambda_n} \frac{r'^{-\Lambda_n} - r'^{-\Lambda(\mathrm{s})}}{\Lambda_n - \Lambda(\mathrm{s})} = -r'^{-\Lambda_n} Ln(r')$$
$$\lim_{\Lambda(\mathrm{s})\to\Lambda_n} \frac{\left(1-\frac{\Lambda_n}{2}\right)r'^{-\Lambda_n} - \left(1-\frac{\Lambda(\mathrm{s})}{2}\right)r'^{-\Lambda(\mathrm{s})}}{\Lambda_n - \Lambda(\mathrm{s})} = \left[\left(\frac{\Lambda_n}{2}-1\right)\mathrm{Ln}(r') - \frac{1}{2}\right]r'^{-\Lambda_n} \quad (52)$$

These expressions have been incorporated into the Mathematica program used for the numerical computations.

7. Numerical applications

In this section, we will show a few numerical examples and parametric studies to illustrate the applicability of the quasi-analytical model and the viscoplastic behaviour described by this model. The data concerning the rock mass are taken from the previous studies (ANDRA, 2005; Bui et al., 2014) which are relative to a deep geological disposal facility for radioactive waste studied in France, and referred to in the following as "reference parameters" (see Table 1).

Table 1. Reference parameters used in the numerical applications

$\alpha = 0.1$; $P_\infty = 12$ MPa; $E = 5000$ MPa; $\nu = 0.5$; $\eta = 2.0 \times 10^{20}$ Pa s; $K_R = 1000$ MPa;
$t_2 = 3804$ years
Leading to:
$K'_R = 0.2$; $T_0 = 1268$ years; $t'_2 = 3$

7.1. Mechanical evolutions of normalized quantities

Figs. 2 and 3 show the variation of normalized radial displacement against normalized time and normalized radial coordinate, respectively. The negative displacement is consistent with an inward movement, due to decompression. Fig. 2 shows that at each location ($r' = 1$, 1.1, 1.3), there is an instantaneous convergence at the initial moment due to excavation. The displacement continues to increase progressively (in absolute value) more or less linearly (exactly linearly at $r' = 1$) with time before the cavity wall comes into contact with the backfill. At time $t' = t'_2$, the cavity wall comes into contact with the backfill and continues to converge at a slower speed due to the confinement effect of the latter. Finally, the cavity wall convergence tends to an asymptotic value, which represents the long-term mechanical equilibrium state. Fig. 3 shows that at any time, the inward

displacement is the largest (in absolute value) at the cavity wall ($r' = 1$) and decreases monotonically to zero towards infinity, which is consistent with the boundary conditions at near and far field. The evolution of convergence at the cavity wall ($r' = 1$) computed numerically using the Stehfest algorithm ($U \approx -7.96$) is also consistent with the exact analytical expression Eq. (C4).

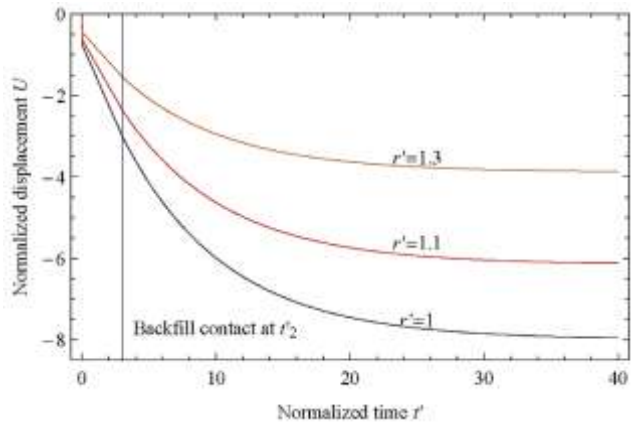

Fig. 2. Temporal evolution of normalized displacement at three different locations ($r' = 1$, 1.1, 1.3).

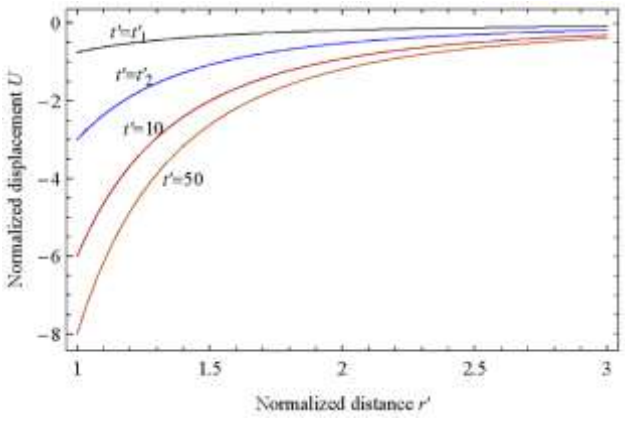

Fig. 3. Normalized displacement profiles at different times ($t' = 0^+(t_1'), 3\ (t_2'), 10, 50$).

Fig. 4 shows the temporal evolution of the total stresses at different radii ($r' = 1$, 1.1, 1.3). The initial jump of stress from the geostatic pressure (-1 for the normalized value at all r') to zero is not shown for clarity. During Stage 2 of free convergence, the radial stresses become more compressive at all radii due to creep effects and the inward convergence so induced, except at the cavity wall, where it remains at zero due to the no-support boundary condition. In the same period, the circumferential stresses also become more compressive due to equilibrium requirements.

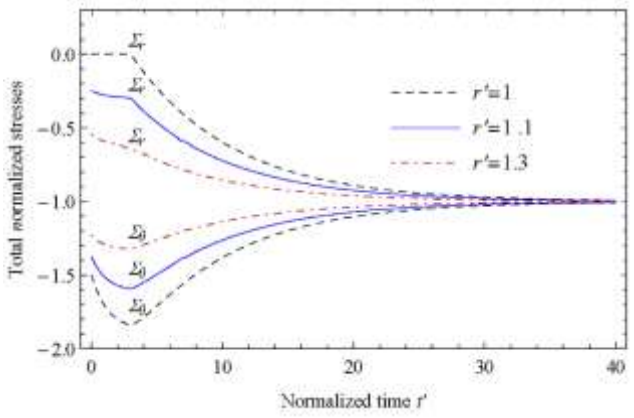

Fig. 4. Temporal evolution of the total stresses at different radii ($r' = 1$, 1.1, 1.3).

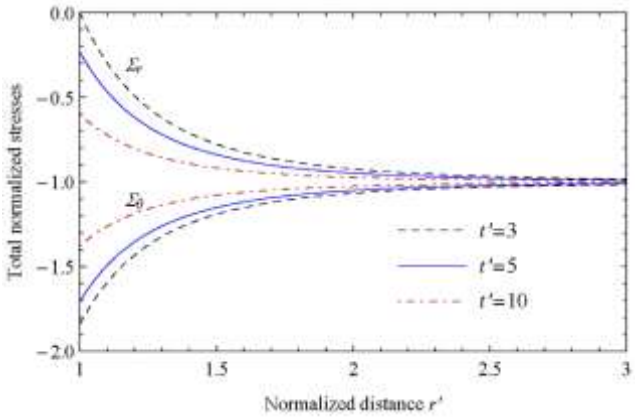

Fig. 5. Profiles of normalized principal total stresses at $t' = t_2' = 3$ (backfill), at $t' = 5$, and at $t' = 10$.

Fig. 5 shows the profiles of normalized stresses at the end of Stage 2, $t' = t_2' = 3$, and at two arbitrary times in Stage 3, $t' = 5$ and $t' = 10$. Both radial and circumferential stresses remain at the geostatic pressure at far field. When going towards the cavity, the radial stress decreases to a minimum while the circumferential stress increases to a maximum at the cavity wall (in absolute value). The radial stress is zero at cavity wall ($r' = 1$) during Stage 2, in accordance with the free convergence

(no-support) assumption. After contact with the backfill (Stage 3, $t' > t'_2$), the radial stress becomes progressively more compressive while the circumferential stress becomes less compressive.

In Stage 3 ($t' > t'_2$), immediately after the contact with the backfill, the rate of change of radial stress (in absolute value) jumps instantly to a higher value while that of the circumferential stress changes sign suddenly (observe the kink at $t' > t'_2$). This discontinuity of the stress rate happens at all radii but is sharper at near field and smoothes out quickly towards the far field. It is due obviously to the confinement effect provided by the backfill. After this initial period, the radial (resp. circumferential) stresses continue to increase (resp. decrease), and both tend asymptotically towards the geostatic pressure.

7.2. Parametric studies

In this section, a few parametric studies will be shown to illustrate their influence on the results of the analytical model. The dilation parameter α and rock viscosity η are two key parameters here. Moreover, backfill stiffness K'_R and the instant of backfill contact t'_2 also influence the structural response. However, a variation of η also affects the time scale (i.e. the normalized time t') via the characteristic relaxation time T_0, which would confuse the observation of the actual effects of this parameter. For this reason, the real time scale will be adopted when showing the influence of η and t'_2.

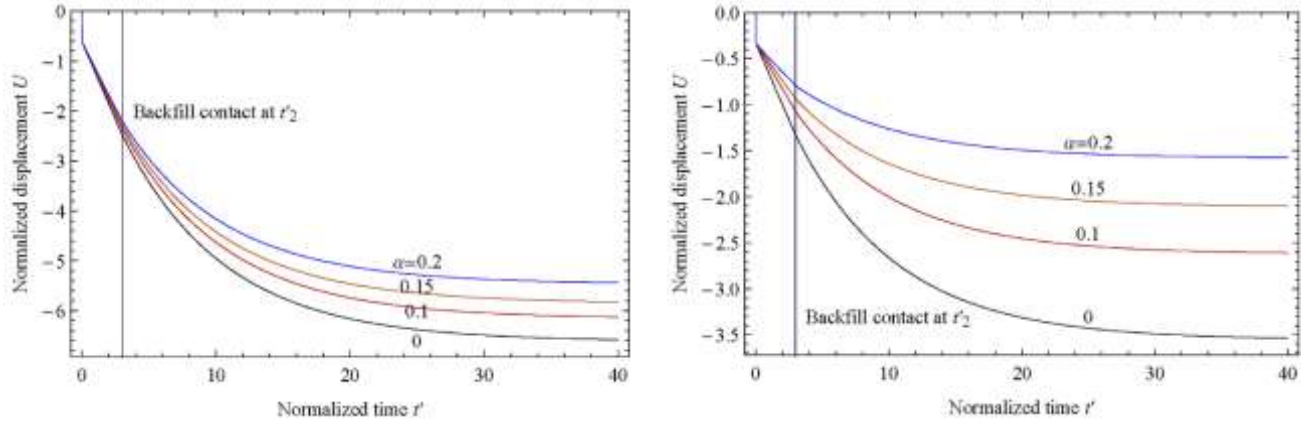

(a) $r' = 1.1$ (b) $r' = 1.5$

Fig. 6. Influence of the dilation parameter on the normalized displacement.

Here again, let us underline that the time evolution of the displacement at the cavity wall ($r' = 1$) is not affected by the dilation parameter α. To study the influence of α on the displacement field, the time evolution of the displacement with different values of α at two other locations ($r' = 1.1$ and $r' = 1.5$) is plotted in Figs. 6. It can be observed that a higher value of α corresponds to a smaller convergence, or in other words, an algebraically larger outward movement. The viscoplastic dilatation is therefore accommodated by an outward movement at every point. This result may surprise. In fact, it is due to the particular symmetry (spherical or cylindrical) involving an infinite domain. This recalls the well-known result (Bérest and Weber, 1998) according to which a linear elastic medium outside a spherical or cylindrical cavity subject to an arbitrary

temperature increase exhibits an outward displacement everywhere except at the cavity wall where the displacement is identically null.

Figs. 7 and 8 show the influence of the dilation parameter α on the normalized radial, circumferential and deviatoric stresses at a point close to the cavity wall ($r' = 1.1$). As expected, the radial and circumferential stresses both become more compressive (i.e. increase in absolute value) with larger values of α since part of the volumetric expansion, incompatible with geometric constraints, has to be absorbed by a stress increase (in compression). Moreover, it can be seen that the circumferential stress is more sensitively affected than the radial one. Fig. 8 shows that the normalized deviatoric stresses (equal to $\Sigma_r - \Sigma_\theta$) increase due to the free convergence till the cavity wall comes into contact with the backfill and then decrease progressively to zero (i.e., the equilibrium mechanical state of the rock mass, since the viscoplastic threshold is null) due to the confinement effect provided by the backfill, and that larger values of α correspond to faster rates of increase and decrease. The peak of deviatoric stress is also higher with larger α.

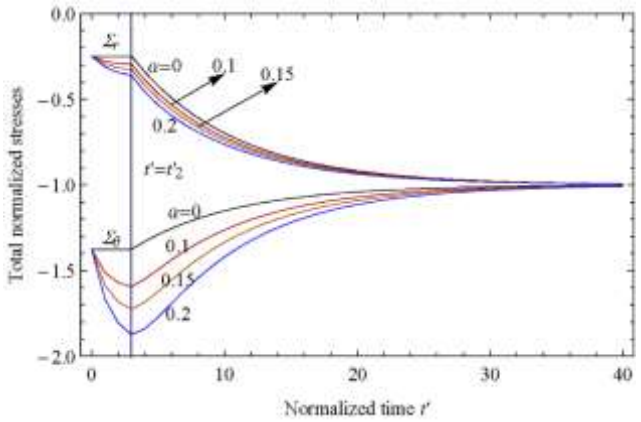

Fig. 7. Normalized total stresses evolution at $r' = 1.1$for different values of dilation parameter α.

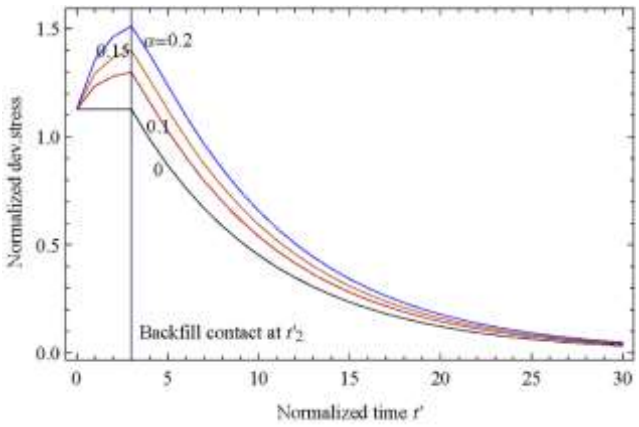

Fig. 8. Profiles of normalized deviatoric stress at $r' = 1.1$with different values of dilation parameter α.

Fig. 9 plots the temporal evolution of normalized deviatoric stress for a particular radius, $r' = 1.1$, for four different normalized backfill stiffness ($K'_R = 0.02, 0.05, 0.1, 0.2$). It can be seen that a stiffer backfill reduces the deviatoric stress, and thus the potential risk of failure.

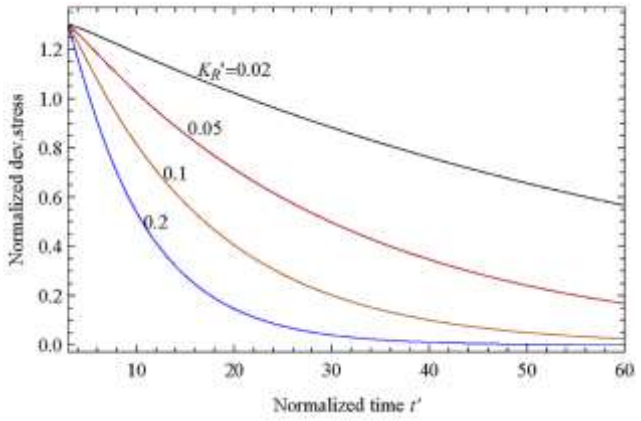

Fig. 9. Influence of the backfill stiffness on the normalized deviatoric stress ($r' = 1.1$).

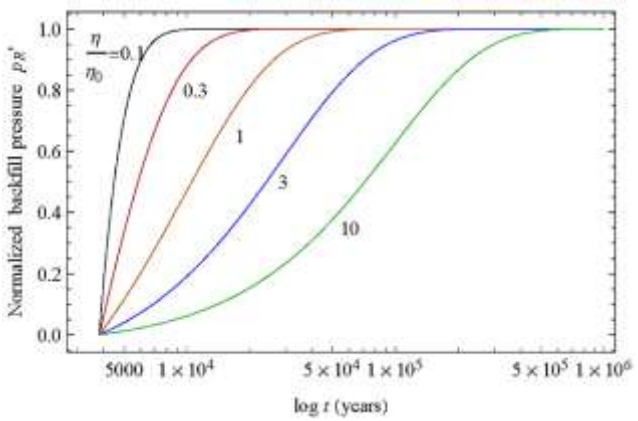

Fig. 10. Temporal evolution of the normalized backfill pressure with different values of rock viscosity.

Fig. 10 represents the temporal evolution of normalized backfill pressure with different values of rock viscosity η. The reference value η_0 (2.0×10^{20} Pa s) listed in Table 1 has been chosen so that creep effects would be significant in order to be well evidenced. It can be found that the backfill pressure tends to geostatic pressure in any case (due to absence of viscoplastic threshold) and that the increase of rock viscosity slows down the rise of backfill pressure. When rock viscosity is infinity (its behaviour then becomes incompressible elastic), the backfill pressure remains zero because in the absence of creep, converging movements of the rock mass stop after excavation. Fig. 11 shows the influence of rock viscosity on normalized convergence in normal time scale and logarithmic time scale. As expected, a larger rock viscosity reduces the equivalent deviatoric plastic strain rate hence the strain at a given time (which can be easily seen from Eq. (10)), thereby reduces the convergence due to creep. When rock viscosity is infinity, the rock mass becomes elastic so no convergence occurs after excavation (absence of Stages 2 and 3).

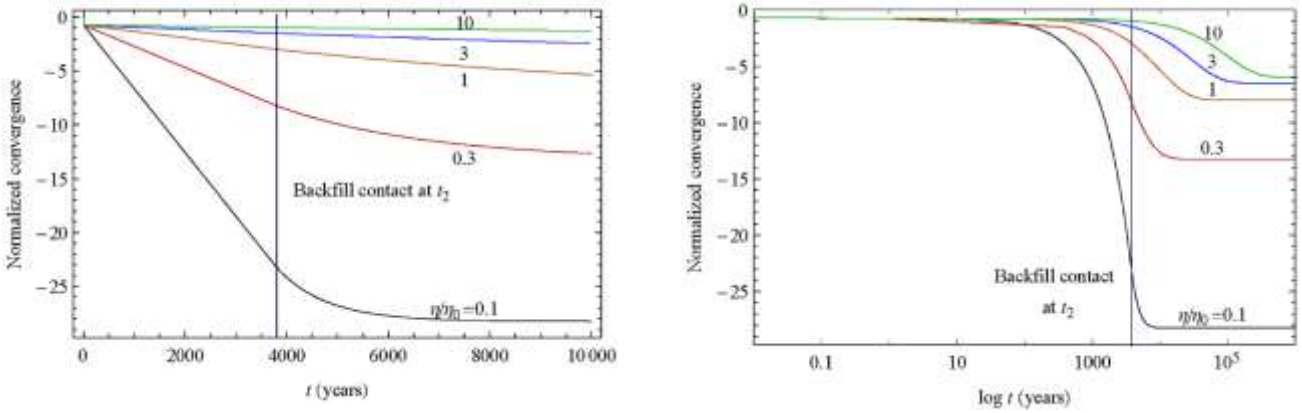

Fig. 11. Evolution of normalized convergence with different viscosities in normal (left) and logarithmic (right) time scales.

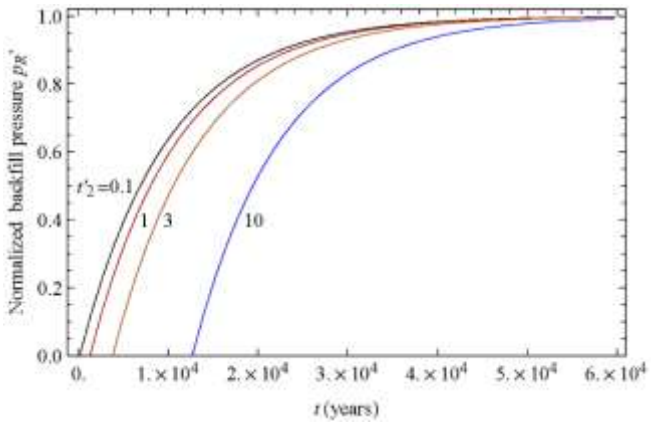

Fig. 12. Influence of the backfill time on the normalized backfill pressure.

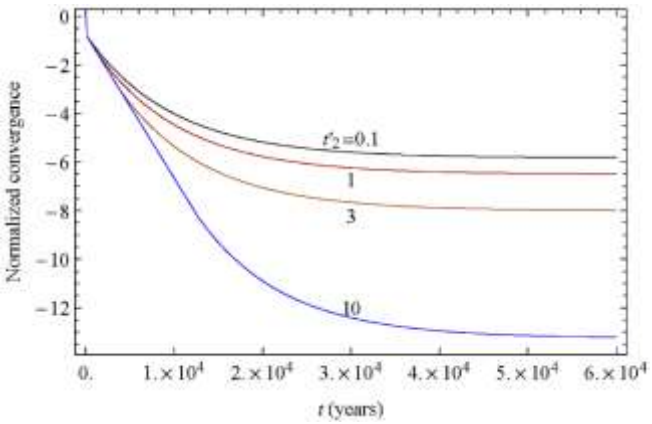

Fig. 13. Influence of the backfill time on the normalized convergence.

Figs. 12 and 13 illustrate the influence of the time t_2 when the cavity wall comes into contact with the backfill on the normalized backfill pressure and on the normalized convergence. Fig. 12 shows that a delayed contact with the backfill can delay the radial stress at the cavity wall. However, this influence declines with time. In other words, the load on filler at larger backfill time t_2 will reach the stable value P_∞ with a faster speed. As expected, Fig. 13 shows that the more the backfill contact time is delayed, the more time of free convergence without support of the cavity wall, thereby induces a larger convergence at any time.

7.3. Comparison with a numerical simulation

Although explicit expressions are obtained for all physical quantities (displacements, stresses, strains), the evaluation of these expressions still needs some light numerical computations, using codes on formal computations such as Mathematical or Maple. It appears judicious to check that these light numerical computations are correctly performed. To this aim, numerical simulations based on FEM have been carried out using COMSOL software (the module on a system of partial differential equations) to solve the system of partial differential equations (14). Only Stages 2 and 3 are modelled since the analytical results in Stage 1 (instantaneous elastic excavation) are trivially classical which provide the initial field values for Stage 2. The results will be presented in normalised forms so that cavity radius will have no influence. In the numerical simulation, the cavity radius was taken to be $r_1 = 5$ m. The backfill ($0 < r < 5$ m) only participates in the third stage of numerical calculation, with a perfect contact assumed with the cavity wall. The problem is defined by two field variables, u and σ_r, which verify two different sets of partial differential equations in the rock mass and backfill. The constitutive behaviour of the latter is assumed to be elastic compressible leading to homogeneous stress and strain fields due to spherical symmetry (Wong et al., 2008a, 2008b).

Fig. 14 shows the 1D finite element mesh used to discretize the interval ($0 < r < 100$ m) in Stage 3. The user-controlled mesh in COMSOL is used in which the maximum element size and maximum element growth rate are respectively set as 0.1 m and 1.2. To minimize edge effects of the external boundary, a large domain for the rock mass is modelled, from $r_1 = 5$ m to

$r_2 = 100$ m. The numerical data used in the simulation are summarized in Table 1. The Poisson's ratio of the backfill is taken as 0.3 (Dufour et al., 2012), and its Young's modulus can therefore be obtained using Eq. (A1).

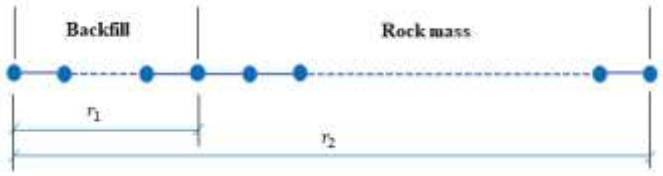

Fig. 14. Finite element mesh of the model in Stage 3.

The main results of the simulation are presented and compared to the quasi-analytical solutions in the following Figs 15, 16, 17 and 18. A good agreement between numerical and analytical results is observed for both Stages 2 and 3.

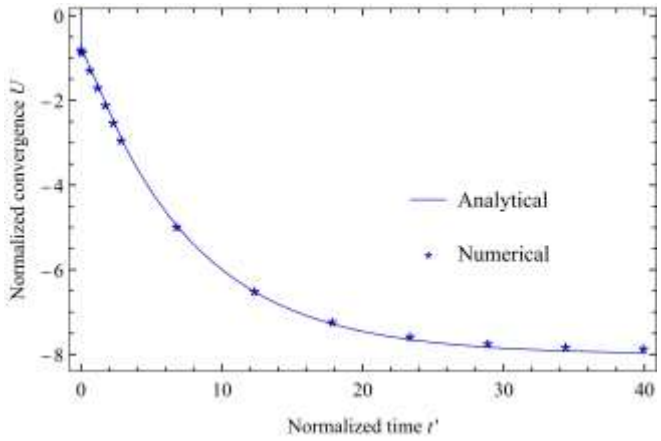

Fig. 15. Temporal evolution of normalized cavity wall convergence.

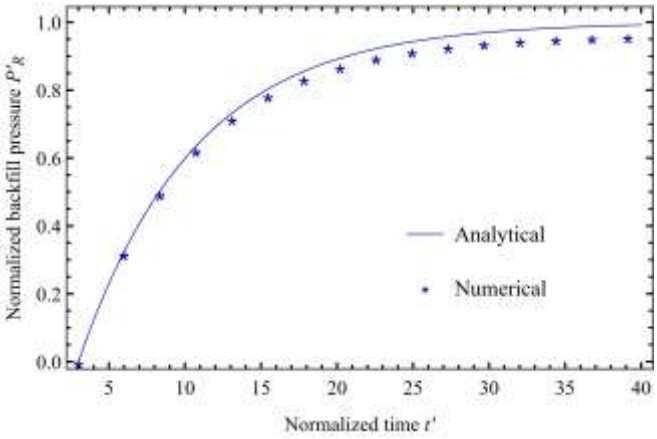

Fig. 16. Temporal evolution of normalized backfill pressure.

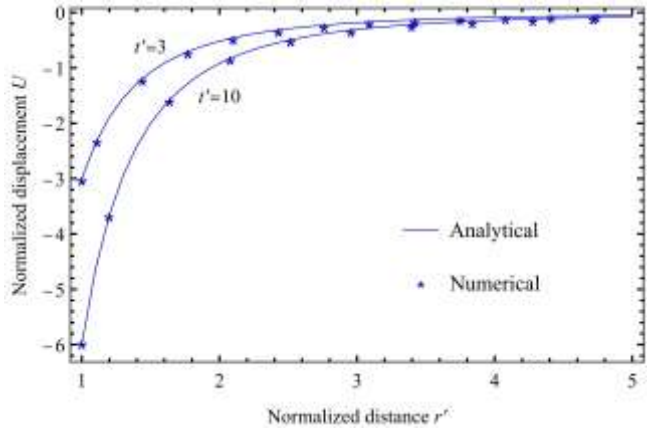

Fig. 17. Profiles of normalized displacement at different times: $t' = 3$ and $t' = 10$.

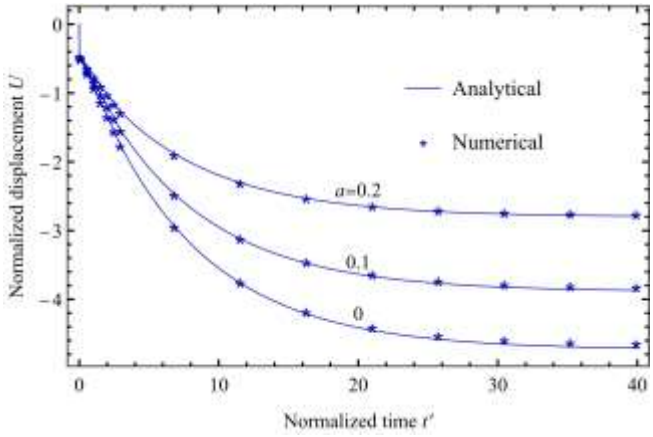

Fig. 18. Temporal evolution of normalized displacement profiles at $r' = 1.3$ with different dilation parameter values.

8. Conclusions

This paper presents a quasi-analytical solution for the post-closure behaviour of a deep cavity excavated inside a dilatant viscoplastic rock mass, accounting for three stages of a simplified life cycle. The present work is an extension of a previous

viscoplastic model with zero dilation. For each stage of the considered life cycle, explicit expressions of displacement and stress fields are deduced in the Laplace transform space. A numerical inversion according to the Stehfest algorithm can then provide the corresponding expressions in time-domain. A few numerical examples and parametric studies are carried out to illustrate the consistency of the solutions and the influence of four key parameters including dilation parameter, rock viscosity, backfill stiffness and the time of backfill contact. Despite some simplifying assumptions adopted to make the problem solvable analytically (elastic incompressibility, linear viscoplastic dilation law, zero creep-threshold...), it provides a valuable tool for checking orders of magnitude at the stage of preliminary studies and also a useful benchmark for validating complex numerical simulations using computer codes.

Declaration of Competing Interest

The authors declare that they have no known competing financial interests or personal relationships that could have appeared to influence the work reported in this paper.

Acknowledgements

The first author is supported by the China Scholarship Council (CSC) with a PhD Scholarship (File No. 202006560007) for his research work.

Appendix A. Derivation of the dimensionless backfill stiffness

We are interested here by the relation between the pressure applied at the exterior surface of a linear elastic solid sphere of radius a, representing the cavity backfill, and its displacement at the same point. Denoting the purely radial displacement inside the backfill by u_R, Eqs. (1)-(3) concerning the form of the strain tensor and the equilibrium equation still apply (replacing u by u_R). Expressing the elastic stresses in terms of displacement using (1) then substituting into equilibrium Eq. (3) leads to the classic Euler's equation: $r^2\partial_{rr}^2 u_R + 2ru_R - 2u_R = 0$. The solution, on account of the zero displacement at the center writes: $u_R(r,t) = U_R(t) * r$, where $U_R(t) = u_R(a,t)/a$ is the dimensionless convergence at the external boundary. Back substitution into Hooke's law gives a homogeneous and isotropic stress field such that $\sigma_r = \sigma_\theta = \frac{E_R}{1-2\nu_R} U_R$, or in rate form: $\dot{\sigma}_r = \dot{\sigma}_\theta = \frac{E_R}{1-2\nu_R}\dot{U}_R$. Since the radial displacement and radial stress are continuous at the backfill-rock mass interface (in terms of rates, due to the difference on the origin of time for the displacement), this implies that the dimensionless convergence of the cavity wall is linearly proportional to the radial ground stress at that point:

$$\dot{\sigma}_r(a,t) = K_R \dot{U}_R(a,t);\ \ K_R = \frac{E_R}{1-2\nu_R} \tag{A1}$$

Normalizing the stress relative to the initial geostatic pressure P_∞ and on account of the normalisation of displacement, we are

led to the following expression of the dimensionless backfill stiffness parameter K'_R appearing in Eq. (37):

$$K'_R = \frac{E_R}{E(1-2\nu_R)} \tag{A2}$$

Appendix B. Consistency of results between Stages 2 and 3

Recalling the time translation $\tau = t' - t'_2$ introduced for Stage 3, and using the classic result of Laplace transform, we have $\Sigma_r(r', t_2'^{+}) = \hat{\Sigma}_r(r', 0^+) = \lim_{s\to\infty} s\,\bar{\Sigma}_r(r', s)$, with $\bar{\Sigma}_r(r', s)$ given by Eq. (47). This leads to:

$$s\,\bar{\Sigma}_r(r', s) = -1 + s\,\gamma(s) r'^{-\Lambda(s)} + \sum_n \frac{s\,B_n(s)}{\Lambda_n - \Lambda(s)}\left(r'^{-\Lambda_n} - r'^{-\Lambda(s)}\right) \tag{B1}$$

It is easy to show that as $s \to \infty$: $\Lambda(s) \to 3$, $s\,\gamma(s) \to 1$, $\frac{s\,B_n(s)}{\Lambda_n - \Lambda(s)} \to \frac{b_n}{\tau_n}$. On account of the identity (36-d):$\sum_{n=1}^{N} \frac{b_n}{\tau_n} = 1$, The above can finally be recast as:

$$\Sigma_r(r', t_2'^{+}) = \lim_{s\to\infty} s\,\bar{\Sigma}_r(r', s) = \sum_n b_n \left(\frac{r'^{-\Lambda_n} - 1}{\tau_n}\right) \tag{B2}$$

However, the above is precisely the numerical inverse Laplace transform of $\frac{r'^{-\Lambda(s)} - 1}{s}$, evaluated at $t' = t'_2$, which corresponds exactly to expression (28). Hence, we have shown that:

$$\Sigma_r(r', t_2'^{+}) = \Sigma_r(r', t_2'^{-}) \tag{B3}$$

in our semi-analytical model.

The proof of the continuity of Σ_θ and U can be easily done following the same steps.

Appendix C. Convergence at cavity wall in Stage 3

At the cavity wall, $r' = 1$, expression (49) simplifies to:

$$\frac{\bar{\bar{U}}}{r'} = -\frac{3(s+1)}{4s}\gamma(s) - \frac{1}{s}\beta(1) \tag{C1}$$

From Eq. (42), and by definition $A^n_{r\theta} = A_r(\tau_n) - A_\theta(\tau_n) = \frac{3\Lambda_n}{4\tau_n^2}$, hence:

$$\beta(1) = \sum_n \frac{b_n A^n_{r\theta}}{\Lambda_n} = \sum_n b_n \frac{3}{4\tau_n^2} \approx \mathcal{L}^{-1}\left[\frac{3}{4s^2}\right]_{t'=t'_2} = \frac{3}{4}t'_2 \tag{C2}$$

On account of the expression (46) of $\gamma(s)$, we get:

$$\bar{\bar{U}}(1, s) = -\frac{3(s+1)}{4s(\omega+s)} - \frac{3t'_2}{4s} \tag{C3}$$

The inversion can be done analytically using partial fractions. It is the same as that of the case $\alpha = 0$ given in Appendix D:

$$U(1, t') = -\frac{3}{4}\left[1 + t'_2 + \left(\frac{1}{\omega} - 1\right)\left(1 - e^{-\omega(t'-t'_2)}\right)\right] \tag{C4}$$

Appendix D. Solution in the case of zero dilatancy ($\alpha = 0$)

Stage 1 ($0 < t' < 0^+$). The quantities after excavation, at $t' = 0^+$, are still given by expressions (20):

Stage 2 ($0^+ < t' < t_2'$). Substituting $\alpha = 0$ into Eqs. (28)-(30), we get:

$$\Sigma_r = -1 + r'^{-3};\ \Sigma_\theta = -1 - \frac{1}{2}r'^{-3};\ U = -\frac{3}{4}\left(1 + t'\right)r'^{-2} \tag{D1}$$

Notice that the stress profiles in Stage 2 in the case of zero dilatancy remain immobile, while the convergence itself increases linearly with time.

Stage 3 ($t_2' < t' < \infty$). When $\alpha = 0$, we have: $\Lambda(s) = \Lambda_n = 3;\ \zeta(r', s) = 0;\ A_{\theta n} = -\frac{A_{rn}}{2} \Rightarrow B_n(s) = 0;\ \beta(r') = \frac{3}{4}t_2' r'^{-3}$, the expressions (47)-(49) then simplifies to (with ω defined in (46)):

$$\overline{\overline{\Sigma_r}} = -\frac{1}{s} + \frac{1}{s+\omega}r'^{-3};\ \overline{\overline{\Sigma_\theta}} = -\frac{1}{s} + \frac{1}{2(s+\omega)}r'^{-3};\ \overline{\overline{U}} = -\frac{3}{4}\left[\frac{s+1}{s(s+\omega)} + \frac{t_2'}{s}\right]r'^{-2} \tag{D2}$$

Analytical inversion yields:

$$\Sigma_r = -1 + e^{-\omega\left(t'-t_2'\right)}r'^{-3};\ \Sigma_\theta = -1 - \frac{1}{2}e^{-\omega\left(t'-t_2'\right)}r'^{-3};\ U = -\frac{3}{4}\left[\frac{1}{\omega} + \left(1 - \frac{1}{\omega}\right)e^{-\omega\left(t'-t_2'\right)} + t_2'\right]r'^{-2} \tag{D3}$$

The solution in this stage can also be obtained by starting anew from (39) with $\alpha = 0$.

References:

Afrouz, A., 1990. Methods to reduce floor heave and sides closure along the arched gate roads. Min. Sci. Technol. 10 (3), 253–263. https://doi.org/10.1016/0167-9031(90)90465-5.

Andra, Dossier 2005 argile. Evaluation de la faisabilité du stockage géologique en formation argileuse'' © Andra; 2005.

Boidy, E., Bouvard, A., Pellet, F., 2002. Back analysis of time-dependent behaviour of a test gallery in claystone. Tunnell. Underg. Space. Technol. 17 (4), 415–424. https://doi.org/10.1016/S0886-7798(02)00066-4.

Bérest, P., Bergues, J., Brouard, B., Durup, J., Guerber, B., 2001. A salt cavern abandonment test. Int. J. Min. Sci. Technol. 38 (3), 357–368. https://doi.org/10.1016/S1365-1609(01)00004-1.

Berest, P., Weber, P.H., 1998. La thermomécanique des roches. https://www.unitheque.com/la-thermomecanique-des-roches/brgm/Livre/12242.

Bui, T.A., Wong, H., Deleruyelle, F., Dufour, N., Leo, C., Sun, D.A., 2014. Analytical modeling of a deep tunnel inside a poro-viscoplastic rock mass accounting for different stages of its life cycle. Comput. Geotech. 58, 88–100. https://doi.org/10.1016/j.compgeo.2013.11.004.

Bui, T.A., Wong, H., Deleruyelle, F., Xie, L.Z., Tran, D.T., 2017. A thermodynamically consistent model accounting for viscoplastic creep and anisotropic damage in unsaturated rocks. Int. J. Solids. Struct. 117, 26–38. https://doi.org/10.1016/j.ijsolstr.2017.04.015.

457 Carranza-Torres, C., Zhao, J., 2009. Analytical and numerical study of the effect of water pressure on the mechanical response of
458 cylindrical lined tunnels in elastic and elasto-plastic porous media. Int. J. Min. Sci. Technol. 46 (3), 531–547.
459 https://doi.org/10.1016/j.ijrmms.2008.09.009.
460 Changa, C., Zoback, M.D., 2009. Viscous creep in room-dried unconsolidated Gulf of Mexico shale (I): Experimental results. J.
461 Petol. Sci. Eng. 69 (3-4), 239–246. https://doi.org/10.1016/j.petrol.2009.08.018.
462 Chiarelli, A., Shao, J., Hoteit, N., 2003. Modelling of elastoplastic damage behaviour of a claystone. Int. J. Plast. 19 (1), 23–45.
463 https://doi.org/10.1016/S0749-6419(01)00017-1.
464 Chijimatsu, M., 2005. Numerical study of the THM effects on the near-field safety of a hypothetical nuclear waste
465 repository—BMT1 of the DECOVALEX III project. Part 1: Conceptualization and characterization of the problems and
466 summary of results. Int. J. Rock Mech. Min. Sci. 42, 720–730. ineris-00175382.
467 Cornet, J.S., Dabrowski, M., 2018. Nonlinear Viscoelastic Closure of Salt Cavities. Rock. Mech. Min. Sci. 103, 96–106.
468 https://doi.org/10.1007/s00603-018-1506-1.
469 Cornet, J.S., Dabrowski, M., Schmid, D.W., 2017. Long-term cavity closure in non-linear rocks. Geophys. J. Int. 210, 1231–
470 1243. https://doi.org/10.1093/gji/ggx227.
471 Cornet, J.S., Dabrowski, M., Schmid, D.W., 2018. Long term creep closure of salt cavities. Int. J. Rock Mech. Min. Sci. 103, 96–
472 106. https://doi.org/10.1016/j.ijrmms.2018.01.025.
473 Cosenza, P., Ghoreychi, M., 1999. Effects of very low permeability on the long-term evolution of a storage cavern in rock salt.
474 Int. J. Min. Sci. Technol. 36, 527–533. https://doi.org/10.1016/S0148-9062(99)00018-2.
475 Dufour, N., Leo, C.J., Wong, H., Deleruyelle, F., 2009. Hydromechanical responses of a decommissioned backfilled tunnel
476 drilled into a poro-viscoelastic medium. Soils. Found. 49 (4), 495–507. https://doi.org/10.3208/sandf.49.495.
477 Dufour, N., Wong, H., Deleruyelle, F., Leo, C.J., 2012. Hydromechanical postclosure behaviour of a deep tunnel taking into
478 account a simplified life cycle. Int. J. Geomech. 12 (5), 549–559. https://doi.org/10.1061/(ASCE)GM.1943-5622.0000126.
479 El Jirari, S., Wong, H., Deleruyelle, F., Branque, D., Berthoz, N., Leo, C., 2020. Analytical modelling of a tunnel accounting for
480 elastoplastic unloading and reloading with reverse yielding and plastic flow. Comput. Geotech. 121, 103441.
481 https://doi.org/10.1016/j.compgeo.2020.103441.
482 Gasc-Barbier, M., Chanchole, S., Berest, P., 2004. Creep behaviour of Bure clayey rock. Appl. Clay. Sci. 26 (1–4), 449–458.
483 https://doi.org/10.1016/j.clay.2003.12.030.
484 Gatelier, N., Pellet, F., Loret, B., 2002. Mechanical damage of an anisotropic porous rock in cyclic triaxial tests. Int. J. Min. Sci.
485 Technol. 39 (3), 335–54. https://doi.org/10.1016/S1365-1609(02)00029-1.
486 Giraud, A., Rousset, G., 1996. Time-dependent behaviour of deep clays. Eng. Geol. 41, 181–95.

https://doi.org/10.1016/0013-7952(95)00000-3.

Hudson, J.A., Stephansson, O., Andersson, J., Tsang, C.F., Jing, J., 2001. Coupled T–H–M issues relating to radioactive waste repository design and performance. Int. J. Min. Sci. Technol. 38 (1), 143–161. https://doi.org/10.1016/S1365-1609(00)00070-8.

Jin, J., Cristescu, N.D., 1998. An elastic/viscoplastic model for transient creep of rock salt. Int. J. Plasticity. 14 (1-3), 85-107. https://doi.org/10.1016/S0749-6419(97)00042-9.

Kazmierczak, J., Laouafa, F., 2007. Ghoreychi M, Lebon P, Barnichon J. Influence of creep on water pressure measured from borehole tests in the Meuse/Haute-Marne Callovo-Oxfordian argillites. Phys. Chem. Earth. 32, 917–921. https://doi.org/10.1016/j.pce.2006.01.008.

Li, L., Chen, H., Li, J., Sun, D., 2021. An elastoplastic solution to undrained expansion of a cylindrical cavity in SANICLAY under plane stress condition. Comput. Geotech. 132, 103990. https://doi.org/10.1016/j.compgeo.2020.103990.

Liedtke, L., Bleich, W., 1985. Convergence calculations for back-filled tunnels in rock salt. Comput. Struct. 21 (1/2), 353–378. https://doi.org/10.1016/0045-7949(85)90255-X.

Lockner, D., 1993. Room temperature creep in saturated granite. J. Geophys. Res. 98 (B1), 475–487. https://doi.org/10.1029/92JB01828.

Malan, D.F., 2002. Simulating the time-dependent behaviour of excavations in hard rock. Rock. Mech. Rock. Eng. 35 (4), 225–254. https://doi.org/10.1007/s00603-002-0026-0.

Nguyen-minh, D., Pouya, A., 1992. A framework for the analysis of underground excavations in viscoplastic medium, on account of a steady stress state. Rev. Franç. Géotech. 59, 5-14. https://doi.org/10.1051/geotech/1992059005.

Pardoen, B., Levasseur, S., Collin, F., 2015. Using Local Second Gradient Model and Shear Strain Localisation to Model the Excavation Damaged Zone in Unsaturated Claystone. Rock. Mech. Rock. Eng. 48(2):691-714. doi: 10.1007/s00603-014-0580-2.

Pardoen, B., Collin, F., 2017. Modelling the influence of strain localisation and viscosity on the behaviour of underground drifts drilled in claystone. Comput. Geotech. 85, 351–367. https://doi.org/10.1016/j.compgeo.2016.05.017.

Pardoen, B., Bésuelle, P., Dal Pont, S., Cosenza, P., Desrues, J., 2020. Accounting for Small-Scale Heterogeneity and Variability of Clay Rock in Homogenised Numerical Micromechanical Response and Microcracking. Rock. Mech. Rock. Eng. 53:2727-2746. doi: 10.1007/s00603-020-02066-7.

Pellet, F., Hajdu, A., Deleruyelle, F., Besnus, F., 2005. A viscoplastic model including anisotropic damage for the time dependent behaviour of rock. Int. J. Numer. Anal. Meth. Geomech. 29, 941–970. https://doi.org/10.1002/nag.450.

Perzyna, P., 1966. Fundamental problems in viscoplasticity. Adv. Appl. Mech. 9, 247–377.

https://doi.org/10.1016/S0065-2156(08)70009-7.

Ribacchi, R., 2000. Mechanical Tests on Pervasively Jointed Rock Material: Insight into Rock Mass Behaviour. Rock. Mech. Rock. Eng. 33, 243–266. https://doi.org/10.1007/s006030070002.

Rutqvist, J., Bäckström, A., Chijimatsu, M., et al. 2009. A multiple-code simulation study of the long-term EDZ evolution of geological nuclear waste repositories. Environ. Geol. 57 (6), 1313–1324. https://doi.org/10.1007/s00254-008-1536-1.

Sekiguchi, H., 1973. Flow characteristics of clays. Soils. Foound. 13 (1), 45–60. https://doi.org/10.3208/sandf1972.13.45.

Stehfest, H., 1970. Algorithm 368. Commun. Assoc. Comput. Mach. 13 (1), 47–49. https://doi.org/10.1145/361953.361969.

Tang, L., Zhao, Y., Liao, J., Liu, Q., 2020. Creep experimental study of rocks containing weak interlayer under multilevel loading and unloading cycles. Front. Earth Sci. 8, Article 519461. https://doi.org/10.3389/feart.2020.519461.

Tian, W.M., Silva, A.J., Veyera, G.E., Sadd, M.H. 1994. Drained creep of undisturbed cohesive marine sediments. Can. Geotech. J. 31 (6), 841–855. https://doi.org/10.1139/t94-101.

Wang, L.Z., Yin, Z.Y., 2015. Stress-dilatancy of natural soft clay under an undrained creep condition. Int. J. Geomech. 15 (5), 1-5. https://doi.org/10.1061/(ASCE)GM.1943-5622.0000271.

Wong, H., Morvan, M., Deleruyelle, F., Leo, C.J., 2008a. Analytical study of mine closure behaviour in a poro-elastic media. Comput. Geotech. 35 (5), 645–654. https://doi.org/10.1016/j.compgeo.2007.11.003.

Wong, H., Morvan, M., Deleruyelle, F., Leo, C.J., 2008b. Analytical study of mine closure behaviour in a poro-viscoelastic medium. Int. J. Numer. Anal. Methods. Geomech. 32 (14), 1737–1761. https://doi.org/10.1002/nag.694.

Yoshinaka, R., Tran, T.V., Osada, M., 1998. Non-linear, stress- and strain-dependent behaviour of soft rocks under cyclic triaxial conditions. Int. J. Rock. Mechines. Min. Sci. 35 (7), 941–955. https://doi.org/10.1016/S0148-9062(98)00158-2.

Yu, H.S., Plasticity and geotechnics. New York, USA: Springer; 2006.

Zhang, C., Czaikowski, O., Rothfuchs, T., Thermo-hydro-mechanical behaviour of the callovo-oxfordian clay rock. Final Report 12/2010; 2010. http://www.grs.de.

Zhao, D., Gao, Q.F., Hattab, M., Hicher, P.Y., Yin, Z.Y., 2020. Microstructural evolution of remolded clay related to creep. Transp. Geotech. 21, 10067. https://doi.org/10.1016/j.trgeo.2020.100367.

Zhou, H., Zhang, K., Feng, X., 2011. Experimental study on progressive yielding of marble. Mater. Res. Innovat. 15 (1), S143–6. https://doi.org/10.1179/143307511X12858956847796.

Zhou, H., Jia, Y., Shao, J.F., 2008. A unified elastic–plastic and viscoplastic damage model for quasi-brittle rocks. Int. J. Rock Mech. Min. Sci. 45, 1237–1251. https://doi.org/10.1016/j.ijrmms.2008.01.004.